IOP Publishing Journal of Physics B: Atomic, Molecular and Optical Physics
J. Phys. B: At. Mol. Opt. Phys. **47** (2014) 085002 (8pp) doi:10.1088/0953-4075/47/8/085002

Single and double photoionization of Ne^{8+}

M S Pindzola[1], Sh A Abdel-Naby[1,2], F Robicheaux[1,3] and J Colgan[4]

[1] Department of Physics, Auburn University, Auburn, AL 36849, USA
[2] Department of Physics, Beni Suef University, Beni Suef, Egypt
[3] Department of Physics, Purdue University, West Lafayette, IN 47907, USA
[4] Theoretical Division, Los Alamos National Laboratory, Los Alamos, NM 87545, USA

E-mail: pindzola@physics.auburn.edu

Received 9 January 2014, revised 7 March 2014
Accepted for publication 13 March 2014
Published 8 April 2014

Abstract

A direct solution of the time-dependent Dirac equation is used to calculate the single and double photoionization cross sections for Ne^{8+}. Expansion of a two-electron wavefunction in coupled spin–orbit eigenfunctions yields time-dependent close-coupled equations for quad-spinor radial wavefunctions. The repulsive interaction between electrons includes both Coulomb and Gaunt interactions. The fully-correlated ground state radial wavefunction is obtained by solving a time-independent inhomogeneous set of close-coupled equations instead of a relaxation of the time-dependent close-coupled equations in imaginary time. A Bessel function expansion is used to include both dipole and quadrupole effects in the radiation field interaction for both the 'velocity' and 'length' gauges. Propagation of the time-dependent close-coupled equations in real time yields single and double photoionization cross sections for Ne^{8+} at energies easily accessible at advanced free electron laser facilities.

Keywords: photoionization, laser, relativistic

1. Introduction

With the continued development of free electron lasers, double photoionization processes will begin to be studied for more highly charged atomic ions where fully relativistic effects will become important. For example, the Free electron LASer at Hamburg (FLASH) at DESY in Hamburg, Germany produces 300 eV photons [1], the Linac Coherent Light Source (LCLS) at SLAC in Menlo Park, California produces 2–10 keV photons [2], and the X-ray Free Electron Laser (XFEL) at DESY in Hamburg, Germany will produce up to 25 keV photons [3].

Relativistic many body perturbation theory has been used for many years to study photon collisions with highly charged atomic ions [4]. Recently fully relativistic perturbation theory calculations reported double to single ratios of total photoionization cross sections for selected He-like atoms up to La^{55+} [5]. Relativistic non-perturbative methods have also been developed to study single photoionization cross sections for arbitrary atoms and ions. These include the Dirac atomic *R*-matrix code method [6], the Dirac B-spline *R*-matrix method [7], and the relativistic converged close-coupling method [8]. The development of the Dirac *R*-matrix with pseudo-states method [9] has allowed for future calculations of non-perturbative double photoionization cross sections for atoms and their ions.

The one-electron time-dependent Dirac equation may be directly solved for single photoionization cross sections for highly charged atomic ions using an eigenstate expansion method [10] or using a time-dependent close-coupling (TDCC-3D) method [11]. For the single photoionization of U^{91+} it was found that the total cross section increased by almost 30% when the electromagnetic field potential was extended to include both dipole and quadrupole effects [11].

The two-electron time-dependent Dirac equation may also be directly solved using a time-dependent close-coupling (TDCC-6D) method [12] for both single and double photoionization cross sections for highly charged atomic ions. In this paper the TDCC-6D method is extended to include multipolar electromagnetic field effects for both electrons and to include electron-electron repulsion effects beyond the standard Coulomb interaction. Single and double photoionization cross sections are calculated for Ne^{8+} over an energy range easily accessible at advanced free electron laser facilities.

The rest of the paper is organized as follows. In section 2.1 we present the two-electron time-dependent Dirac equation in

both the 'velocity' and 'length' gauges with both Coulomb and Gaunt two-body interactions. In section 2.2 we present the TDCC-6D equations in terms of matrix elements between two electron jjJ coupled states for the electromagnetic field potentials and the two-body repulsion operators. In section 2.3 and appendix we reduce the matrix elements for the electromagnetic field and the two-body repulsion operators to time-dependent radial operators and standard nj symbols. In section 2.4 we present the two-electron time-dependent inhomogeneous Dirac equation needed to obtain the fully correlated ground state wavefunction. In section 2.5 we present the initial time boundary conditions and the final time probability scattering amplitudes and cross sections. In section 3 we present computational details on the numerical lattice solutions of the TDCC-6D equations and single and double photoionization cross sections for Ne^{8+}. In section 4 we conclude with a summary and an outlook for future work. Unless otherwise stated, all quantities are given in atomic units.

2. Theory

2.1. Time-dependent Dirac equation

The time-dependent Dirac equation for a two-electron atomic ion in a time-varying electromagnetic field is given by [13, 14]:

$$\mathrm{i}\frac{\partial\vec{\Psi}(\vec{r}_1,\vec{r}_2,t)}{\partial t} = \bar{H}(\vec{r}_1,\vec{r}_2,t)\vec{\Psi}(\vec{r}_1,\vec{r}_2,t), \tag{1}$$

where

$$\bar{H}(\vec{r}_1,\vec{r}_2,t) = \begin{pmatrix} H(\vec{r}_1,\vec{r}_2,t) & c\vec{\sigma}\cdot(\vec{p}_1+\vec{A}_1(t)) & c\vec{\sigma}\cdot(\vec{p}_2+\vec{A}_2(t)) & G(\vec{r}_1,\vec{r}_2) \\ c\vec{\sigma}\cdot(\vec{p}_1+\vec{A}_1(t)) & H(\vec{r}_1,\vec{r}_2,t)-2c^2 & G(\vec{r}_1,\vec{r}_2) & c\vec{\sigma}\cdot(\vec{p}_2+\vec{A}_2(t)) \\ c\vec{\sigma}\cdot(\vec{p}_2+\vec{A}_2(t)) & G(\vec{r}_1,\vec{r}_2) & H(\vec{r}_1,\vec{r}_2,t)-2c^2 & c\vec{\sigma}\cdot(\vec{p}_1+\vec{A}_1(t)) \\ G(\vec{r}_1,\vec{r}_2) & c\vec{\sigma}\cdot(\vec{p}_2+\vec{A}_2(t)) & c\vec{\sigma}\cdot(\vec{p}_1+\vec{A}_1(t)) & H(\vec{r}_1,\vec{r}_2,t)-4c^2 \end{pmatrix} \tag{2}$$

and

$$H(\vec{r}_1,\vec{r}_2,t) = \sum_{i=1}^{2}\left(-\frac{Z}{r_i}-U_i(t)\right)+C(\vec{r}_1,\vec{r}_2). \tag{3}$$

In equations (1)–(3), Z is the atomic number, $\vec{\sigma}$ is a Pauli matrix vector, and $\vec{p}=-i\nabla$ is the momentum operator. In the 'velocity' gauge the electromagnetic field potentials are given by:

$$\begin{aligned} U(t) &= 0, \\ \vec{A}(t) &= \frac{E}{\omega}\hat{z}\sin\left(\frac{\omega}{c}y-\omega t\right), \end{aligned} \tag{4}$$

while in the 'length' gauge the electromagnetic field potentials are given by:

$$\begin{aligned} U(t) &= -Ez\cos(\omega t), \\ \vec{A}(t) &= \frac{E}{\omega}\hat{z}\sin\left(\frac{\omega}{c}y-\omega t\right)+\frac{E}{\omega}\hat{z}\sin(\omega t), \end{aligned} \tag{5}$$

where E is the radiation field amplitude, ω is the radiation field frequency, and c is the speed of light (see chapter 13, complement A) [15]. The two-body Coulomb interaction is given by:

$$C(\vec{r}_1,\vec{r}_2) = \frac{1}{|\vec{r}_1-\vec{r}_2|}, \tag{6}$$

while the two-body Gaunt interaction [16] is given by:

$$G(\vec{r}_1,\vec{r}_2) = -\frac{\vec{\sigma}_1\cdot\vec{\sigma}_2}{|\vec{r}_1-\vec{r}_2|}, \tag{7}$$

(see chapter 6, section 4) [4]. The Gaunt interaction is the unretarded interaction between two Dirac currents, while an additional retarded interaction was added by Breit [14]. The unretarded interaction dominates the correction to the two-body Coulomb interaction [17].

2.2. Time-dependent close-coupled quad-spinor equations

The two-electron total wavefunction is expanded in coupled spin–orbit eigenfunctions given by:

$$\vec{\Psi}(\vec{r}_1,\vec{r}_2,t) = \begin{pmatrix} \sum_{j_1,j_2}\frac{PP^{JM}_{\kappa_1\kappa_2}(r_1,r_2,t)}{r_1r_2}\sum_{m_1,m_2}C^{j_1j_2J}_{m_1m_2M}\Phi_{+\kappa_1,m_1}(\theta_1,\phi_1)\Phi_{+\kappa_2,m_2}(\theta_2,\phi_2) \\ \mathrm{i}\sum_{j_1,j_2}\frac{QP^{JM}_{\kappa_1\kappa_2}(r_1,r_2,t)}{r_1r_2}\sum_{m_1,m_2}C^{j_1j_2J}_{m_1m_2M}\Phi_{-\kappa_1,m_1}(\theta_1,\phi_1)\Phi_{+\kappa_2,m_2}(\theta_2,\phi_2) \\ \mathrm{i}\sum_{j_1,j_2}\frac{PQ^{JM}_{\kappa_1\kappa_2}(r_1,r_2,t)}{r_1r_2}\sum_{m_1,m_2}C^{j_1j_2J}_{m_1m_2M}\Phi_{+\kappa_1,m_1}(\theta_1,\phi_1)\Phi_{-\kappa_2,m_2}(\theta_2,\phi_2) \\ \sum_{j_1,j_2}\frac{QQ^{JM}_{\kappa_1\kappa_2}(r_1,r_2,t)}{r_1r_2}\sum_{m_1,m_2}C^{j_1j_2J}_{m_1m_2M}\Phi_{-\kappa_1,m_1}(\theta_1,\phi_1)\Phi_{-\kappa_2,m_2}(\theta_2,\phi_2) \end{pmatrix}, \tag{8}$$

where the spin–orbit eigenfunctions are given by:

$$\Phi_{\kappa m}(\theta,\phi) = \sum_{m_l,m_s}C^{lsj}_{m_lm_sm_j}Y_{lm_l}(\theta,\phi)\chi_{m_s}, \tag{9}$$

$\kappa=-(l+1)$ for $j=l+\frac{1}{2}$, $\kappa=+l$ for $j=l-\frac{1}{2}$, $s=\frac{1}{2}$, $C^{lsj}_{m_lm_sm_j}$ and $C^{j_1j_2J}_{m_1m_2M}$ are Clebsch–Gordan coefficients, $Y_{lm_l}(\theta,\phi)$ is a spherical harmonic, and χ_{m_s} is a two component spinor. Substitution of equation (8) into the time-dependent Dirac equation of equation (1) and projection onto jjJ coupled spin–orbit eigenfunctions yields the following set of time-dependent close-coupled partial differential equations:

$$\begin{aligned} \mathrm{i}\frac{\partial PP^{JM}_{\kappa_1\kappa_2}(r_1,r_2,t)}{\partial t} &= \left(-\frac{Z}{r_1}-\frac{Z}{r_2}\right)PP^{JM}_{\kappa_1\kappa_2}(r_1,r_2,t) \\ &-c\left(\frac{\partial}{\partial r_1}-\frac{\kappa_1}{r_1}\right)QP^{JM}_{\kappa_1\kappa_2}(r_1,r_2,t) \\ &-c\left(\frac{\partial}{\partial r_2}-\frac{\kappa_2}{r_2}\right)PQ^{JM}_{\kappa_1\kappa_2}(r_1,r_2,t) \\ &-\sum_{J',M'}\sum_{\kappa_1',\kappa_2'}\langle(\kappa_1,\kappa_2)JM|U_1(t) \\ &+U_2(t)|(\kappa_1',\kappa_2')J'M'\rangle PP^{J'M'}_{\kappa_1'\kappa_2'}(r_1,r_2,t) \\ &+\mathrm{i}c\sum_{J',M'}\sum_{\kappa_1',\kappa_2'}\langle(\kappa_1,\kappa_2)JM|\vec{\sigma}\cdot\vec{A}_1(t) \\ &\times|(-\kappa_1',\kappa_2')J'M'\rangle QP^{J'M'}_{\kappa_1'\kappa_2'}(r_1,r_2,t) \\ &+\mathrm{i}c\sum_{J',M'}\sum_{\kappa_1',\kappa_2'}\langle(\kappa_1,\kappa_2)JM|\vec{\sigma}\cdot\vec{A}_2(t) \\ &\times|(\kappa_1',-\kappa_2')J'M'\rangle PQ^{J'M'}_{\kappa_1'\kappa_2'}(r_1,r_2,t) \\ &+\sum_{J',M'}\sum_{\kappa_1',\kappa_2'}\langle(\kappa_1,\kappa_2)JM|C(\vec{r}_1,\vec{r}_2) \\ &\times|(\kappa_1',\kappa_2')J'M'\rangle PP^{J'M'}_{\kappa_1'\kappa_2'}(r_1,r_2,t) \\ &+\sum_{J',M'}\sum_{\kappa_1',\kappa_2'}\langle(\kappa_1,\kappa_2)JM|G(\vec{r}_1,\vec{r}_2) \\ &\times|(-\kappa_1',-\kappa_2')J'M'\rangle QQ^{J'M'}_{\kappa_1'\kappa_2'}(r_1,r_2,t) \end{aligned} \tag{10}$$

$$
\begin{aligned}
\mathrm{i}\frac{\partial QP^{JM}_{\kappa_1\kappa_2}(r_1,r_2,t)}{\partial t} &= \left(-\frac{Z}{r_1}-\frac{Z}{r_2}-2c^2\right)QP^{JM}_{\kappa_1\kappa_2}(r_1,r_2,t)\\
&+c\left(\frac{\partial}{\partial r_1}+\frac{\kappa_1}{r_1}\right)PP^{JM}_{\kappa_1\kappa_2}(r_1,r_2,t)\\
&+c\left(\frac{\partial}{\partial r_2}-\frac{\kappa_2}{r_2}\right)QQ^{JM}_{\kappa_1\kappa_2}(r_1,r_2,t)\\
&-\sum_{J',M'}\sum_{\kappa_1',\kappa_2'}\langle(-\kappa_1,\kappa_2)JM|U_1(t)\\
&+U_2(t)|(-\kappa_1',\kappa_2')J'M'\rangle QP^{J'M'}_{\kappa_1'\kappa_2'}(r_1,r_2,t)\\
&-\mathrm{i}c\sum_{J',M'}\sum_{\kappa_1',\kappa_2'}\langle(-\kappa_1,\kappa_2)JM|\vec{\sigma}\cdot\vec{A}_1(t)\\
&\times|(\kappa_1',\kappa_2')J'M'\rangle PP^{J'M'}_{\kappa_1'\kappa_2'}(r_1,r_2,t)\\
&-\mathrm{i}c\sum_{J',M'}\sum_{\kappa_1',\kappa_2'}\langle(-\kappa_1,\kappa_2)JM|\vec{\sigma}\cdot\vec{A}_2(t)\\
&\times|(-\kappa_1',-\kappa_2')J'M'\rangle QQ^{J'M'}_{\kappa_1'\kappa_2'}(r_1,r_2,t)\\
&+\sum_{J',M'}\sum_{\kappa_1',\kappa_2'}\langle(-\kappa_1,\kappa_2)JM|C(\vec{r}_1,\vec{r}_2)\\
&\times|(-\kappa_1',\kappa_2')J'M'\rangle QP^{J'M'}_{\kappa_1'\kappa_2'}(r_1,r_2,t)\\
&+\sum_{J',M'}\sum_{\kappa_1',\kappa_2'}\langle(-\kappa_1,\kappa_2)JM|G(\vec{r}_1,\vec{r}_2)\\
&\times|(\kappa_1',-\kappa_2')J'M'\rangle PQ^{J'M'}_{\kappa_1'\kappa_2'}(r_1,r_2,t) \qquad (11)
\end{aligned}
$$

$$
\begin{aligned}
\mathrm{i}\frac{\partial PQ^{JM}_{\kappa_1\kappa_2}(r_1,r_2,t)}{\partial t} &= \left(-\frac{Z}{r_1}-\frac{Z}{r_2}-2c^2\right)PQ^{JM}_{\kappa_1\kappa_2}(r_1,r_2,t)\\
&+c\left(\frac{\partial}{\partial r_1}-\frac{\kappa_1}{r_1}\right)QQ^{JM}_{\kappa_1\kappa_2}(r_1,r_2,t)\\
&+c\left(\frac{\partial}{\partial r_2}+\frac{\kappa_2}{r_2}\right)PP^{JM}_{\kappa_1\kappa_2}(r_1,r_2,t)\\
&-\sum_{J',M'}\sum_{\kappa_1',\kappa_2'}\langle(\kappa_1,-\kappa_2)JM|U_1(t)\\
&+U_2(t)|(\kappa_1',-\kappa_2')J'M'\rangle PQ^{J'M'}_{\kappa_1'\kappa_2'}(r_1,r_2,t)\\
&-\mathrm{i}c\sum_{J',M'}\sum_{\kappa_1',\kappa_2'}\langle(\kappa_1,-\kappa_2)JM|\vec{\sigma}\cdot\vec{A}_1(t)\\
&\times|(-\kappa_1',-\kappa_2')J'M'\rangle QQ^{J'M'}_{\kappa_1'\kappa_2'}(r_1,r_2,t)\\
&-\mathrm{i}c\sum_{J',M'}\sum_{\kappa_1',\kappa_2'}\langle(\kappa_1,-\kappa_2)JM|\vec{\sigma}\cdot\vec{A}_2(t)\\
&\times|(\kappa_1',\kappa_2')J'M'\rangle PP^{J'M'}_{\kappa_1'\kappa_2'}(r_1,r_2,t)\\
&+\sum_{J',M'}\sum_{\kappa_1',\kappa_2'}\langle(\kappa_1,-\kappa_2)JM|C(\vec{r}_1,\vec{r}_2)\\
&\times|(\kappa_1',-\kappa_2')J'M'\rangle PQ^{J'M'}_{\kappa_1'\kappa_2'}(r_1,r_2,t)\\
&+\sum_{J',M'}\sum_{\kappa_1',\kappa_2'}\langle(\kappa_1,-\kappa_2)JM|G(\vec{r}_1,\vec{r}_2)\\
&\times|(-\kappa_1',\kappa_2')J'M'\rangle QP^{J'M'}_{\kappa_1'\kappa_2'}(r_1,r_2,t) \qquad (12)
\end{aligned}
$$

$$
\begin{aligned}
\mathrm{i}\frac{\partial QQ^{JM}_{\kappa_1\kappa_2}(r_1,r_2,t)}{\partial t} &= \left(-\frac{Z}{r_1}-\frac{Z}{r_2}-4c^2\right)QQ^{JM}_{\kappa_1\kappa_2}(r_1,r_2,t)\\
&-c\left(\frac{\partial}{\partial r_1}+\frac{\kappa_1}{r_1}\right)PQ^{JM}_{\kappa_1\kappa_2}(r_1,r_2,t)\\
&-c\left(\frac{\partial}{\partial r_2}+\frac{\kappa_2}{r_2}\right)QP^{JM}_{\kappa_1\kappa_2}(r_1,r_2,t)\\
&-\sum_{J',M'}\sum_{\kappa_1',\kappa_2'}\langle(-\kappa_1,-\kappa_2)JM|U_1(t)\\
&+U_2(t)|(-\kappa_1',-\kappa_2')J'M'\rangle QQ^{J'M'}_{\kappa_1'\kappa_2'}(r_1,r_2,t)\\
&+\mathrm{i}c\sum_{J',M'}\sum_{\kappa_1',\kappa_2'}\langle(-\kappa_1,-\kappa_2)JM|\vec{\sigma}\cdot\vec{A}_1(t)\\
&\times|(\kappa_1',-\kappa_2')J'M'\rangle PQ^{J'M'}_{\kappa_1'\kappa_2'}(r_1,r_2,t)\\
&+\mathrm{i}c\sum_{J',M'}\sum_{\kappa_1',\kappa_2'}\langle(-\kappa_1,-\kappa_2)JM|\vec{\sigma}\cdot\vec{A}_2(t)\\
&\times|(-\kappa_1',\kappa_2')J'M'\rangle QP^{J'M'}_{\kappa_1'\kappa_2'}(r_1,r_2,t)\\
&+\sum_{J',M'}\sum_{\kappa_1',\kappa_2'}\langle(-\kappa_1,-\kappa_2)JM|C(\vec{r}_1,\vec{r}_2)\\
&\times|(-\kappa_1',-\kappa_2')J'M'\rangle QQ^{J'M'}_{\kappa_1'\kappa_2'}(r_1,r_2,t)\\
&+\sum_{J',M'}\sum_{\kappa_1',\kappa_2'}\langle(-\kappa_1,-\kappa_2)JM|G(\vec{r}_1,\vec{r}_2)\\
&\times|(\kappa_1',\kappa_2')J'M'\rangle PP^{J'M'}_{\kappa_1'\kappa_2'}(r_1,r_2,t). \qquad (13)
\end{aligned}
$$

2.3. Matrix elements

The radiation field matrix elements found in the close-coupled equations may involve the operators: $U(t) = -Ez\cos(\omega t)$, $\vec{\sigma}\cdot\vec{A}(t) = \frac{E}{\omega}\sin(\omega t)$, and $\vec{\sigma}\cdot\vec{A}(t) = \frac{E}{\omega}\sin(\frac{\omega}{c}y-\omega t)$, depending on the choice of gauge found in equations (4) and (5). Matrix elements involving $\sin(\frac{\omega}{c}y-\omega t)$ may be obtained using the spherical Bessel function expansion given by:

$$
\begin{aligned}
&\sin\left(\frac{\omega}{c}y-\omega t\right)\\
&=\mathrm{Im}\left(\sum_{k,q}i^k(2k+1)C^{k*}_q(\hat{y})\,j_k\left(\frac{\omega}{c}r\right)C^k_q(\hat{r})\,\mathrm{e}^{-i\omega t}\right), \qquad (14)
\end{aligned}
$$

where C^k_q is a spherical tensor operator and $j_k(\frac{\omega}{c}r)$ is a spherical Bessel function. The first two terms in the operator expansion are given by:

$$
\begin{aligned}
\vec{\sigma}\cdot\vec{A}(t) &= -\frac{E}{\omega}\sin(\omega t)\left[j_0\left(\frac{\omega}{c}r\right)\sigma_z C^0_0\right.\\
&\left.-3j_1\left(\frac{\omega}{c}r\right)\sigma_z\left(C^1_{+1}+C^1_{-1}\right)\right]. \qquad (15)
\end{aligned}
$$

For ease in the evaluation of matrix elements we make use of the tensor operator $V(k)^K_Q = (C^k\times S^1)^K_Q$ such that the first two terms in the operator expansion are given by:

$$
\begin{aligned}
\vec{\sigma}\cdot\vec{A}(t) &= -2\frac{E}{\omega}\sin(\omega t)\left[j_0\left(\frac{\omega}{c}r\right)V(0)^1_0\right.\\
&\left.-3j_1\left(\frac{\omega}{c}r\right)\frac{1}{2}\left(V(1)^2_{+1}+V(1)^2_{-1}-V(1)^1_{+1}+V(1)^1_{-1}\right)\right]. \qquad (16)
\end{aligned}
$$

Additional terms involving higher order spherical Bessel functions in either equation (15) or equation (16) may be easily obtained.

Using $\sigma_z = 2S_0^1$, in lowest order for the 'velocity' gauge: $U(t) = 0$ and

$$\vec{\sigma} \cdot \vec{A}(t) = -2\frac{E}{\omega} \sin(\omega t) j_0\left(\frac{\omega}{c} r\right) S_0^1. \tag{17}$$

Using $z = rC_0^1$, in lowest order for the 'length' gauge: $U(t) = -Er\cos(\omega t)C_0^1$ and

$$\vec{\sigma} \cdot \vec{A}(t) = -2\frac{E}{\omega} \sin(\omega t) \left(j_0\left(\frac{\omega}{c} r\right) - 1\right) S_0^1. \tag{18}$$

We note that $j_0(\frac{\omega}{c} r) \approx 1$ for low frequencies.

Matrix elements may be evaluated by standard algebraic reduction of the tensor operators S_0^1, C_0^1, and $V(k)_Q^K$ between $|(\kappa_1, \kappa_2)JM >= |(l_1 \tfrac{1}{2} j_1, l_2 \tfrac{1}{2} j_2)JM >$ coupled states (see chapter 11) [18], as found in the appendix (equations (A.1)–(A.6)).

The two-body Coulomb and Gaunt interactions may be expanded in terms of tensor operators given by:

$$C(\vec{r}_1, \vec{r}_2) = \sum_\lambda \frac{r_<^\lambda}{r_>^{\lambda+1}} C^\lambda(1) \cdot C^\lambda(2) \tag{19}$$

and

$$G(\vec{r}_1, \vec{r}_2) = 4 \sum_{\lambda,K} (-1)^{\lambda+K} \frac{r_<^\lambda}{r_>^{\lambda+1}} V(\lambda)^K(1) \cdot V(\lambda)^K(2), \tag{20}$$

where $r_< = \min(\mathrm{r}_1, \mathrm{r}_2)$ and $r_> = \max(\mathrm{r}_1, \mathrm{r}_2)$. Matrix elements may be evaluated by standard algebraic reduction of the tensor operators C^λ and $V(\lambda)^K$ between coupled states (see chapter 11) [18], as found in the appendix (equations (A.7) and (A.8)).

2.4. Correlated initial state wavefunction

The fully correlated ground state wavefunction cannot be obtained by relaxation of the close-coupled equations associated with the Dirac equation in imaginary time given by:

$$-\frac{\partial \vec{\Psi}(\vec{r}_1, \vec{r}_2, \tau)}{\partial \tau} = \bar{H}(\vec{r}_1, \vec{r}_2) \vec{\Psi}(\vec{r}_1, \vec{r}_2, \tau), \tag{21}$$

where $\bar{H}(\vec{r}_1, \vec{r}_2)$ is found from equation (2) with $U_i(t) = 0$ and $\vec{A}_i(t) = 0$, due to the underlying Dirac sea of negative energy solutions. An approximate method, that we have used previously [12], is to relax the close-coupled equations associated with the 'squared' Dirac equation in imaginary time given by:

$$-\frac{\partial \vec{\Psi}(\vec{r}_1, \vec{r}_2, \tau)}{\partial \tau} = \bar{H}(\vec{r}_1, \vec{r}_2) \bar{H}(\vec{r}_1, \vec{r}_2) \vec{\Psi}(\vec{r}_1, \vec{r}_2, \tau). \tag{22}$$

Although fairly accurate, relaxation of the 'squared' Dirac equation yields an initial state solution that produces unphysical flow patterns in the time propagation of equations (10)–(13). However, the overall effect on the final total cross sections is fairly small.

An exact method is to solve the close-coupled equations associated with an inhomogeneous Dirac equation in real time given by:

$$\mathrm{i}\frac{\partial \vec{\Psi}(\vec{r}_1, \vec{r}_2, t)}{\partial t} = (\bar{H}(\vec{r}_1, \vec{r}_2) - E_0) \vec{\Psi}(\vec{r}_1, \vec{r}_2, t) + \sin^2\left(\frac{\pi t}{T_0}\right) \vec{\Psi}_0(\vec{r}_1, \vec{r}_2), \tag{23}$$

where $\vec{\Psi}(\vec{r}_1, \vec{r}_2, t = 0) = 0$, $\vec{\Psi}_0(\vec{r}_1, \vec{r}_2)$ is an approximate ground state solution with energy E_0, the homing time $T_0 > 10/\Delta E$, and ΔE is the energy difference between the ground and first excited state. The method has been used before to home in on specific Rydberg state solutions of the Schrodinger equation near the ionization limit [19]. The homing of the Dirac equation yields a solution that produces completely clean flow patterns in the time propagation of equations (10)–(13), in keeping with the attainment of an exact solution on the chosen numerical lattice. We also note that the homing method is easier to implement than the iterative damping relaxation method used for many years in relativistic heavy ion collision calculations [20].

2.5. Initial conditions and cross sections

The initial condition for the solution of the time-dependent close-coupled equations (10)– (13) for the photoionization of the fully correlated ground state ($J = 0, M = 0$) is given by:

$$PP^{JM}_{\kappa_1\kappa_2}(r_1, r_2, t = 0) = \sum_\kappa PP^{00}_{\kappa\kappa}(r_1, r_2) \delta_{\kappa_1,\kappa} \delta_{\kappa_2,\kappa} \delta_{J,0} \delta_{M,0} \tag{24}$$

$$QP^{JM}_{\kappa_1\kappa_2}(r_1, r_2, t = 0) = \sum_\kappa QP^{00}_{\kappa\kappa}(r_1, r_2) \delta_{\kappa_1,\kappa} \delta_{\kappa_2,\kappa} \delta_{J,0} \delta_{M,0} \tag{25}$$

$$PQ^{JM}_{\kappa_1\kappa_2}(r_1, r_2, t = 0) = \sum_\kappa PQ^{00}_{\kappa\kappa}(r_1, r_2) \delta_{\kappa_1,\kappa} \delta_{\kappa_2,\kappa} \delta_{J,0} \delta_{M,0} \tag{26}$$

$$QQ^{JM}_{\kappa_1\kappa_2}(r_1, r_2, t = 0) = \sum_\kappa QQ^{00}_{\kappa\kappa}(r_1, r_2) \delta_{\kappa_1,\kappa} \delta_{\kappa_2,\kappa} \delta_{J,0} \delta_{M,0}, \tag{27}$$

where the radial wavefunctions, $PP^{00}_{\kappa\kappa}(r_1, r_2)$, $QP^{00}_{\kappa\kappa}(r_1, r_2)$, $PQ^{00}_{\kappa\kappa}(r_1, r_2)$, and $QQ^{00}_{\kappa\kappa}(r_1, r_2)$ are obtained using the close-coupled equations associated with the inhomogeneous Dirac equation.

Following time propagation of the close-coupled equations (10)–(13) with the initial conditions of equations (24)–(27), the single photoionization probability, leaving the ion in state $n_1\kappa_1$ is given by:

$$\begin{aligned}
\mathcal{P}_s(n_1\kappa_1) = 2 \sum_M \sum_{\epsilon_2\kappa_2} | & \int_0^\infty \mathrm{d}r_1 \int_0^\infty \mathrm{d}r_2 P_{n_1\kappa_1}(r_1) \\
& \times P_{\epsilon_2\kappa_2}(r_2) PP^{1M}_{\kappa_1\kappa_2}(r_1, r_2, t \to \infty) \\
& + \int_0^\infty \mathrm{d}r_1 \int_0^\infty \mathrm{d}r_2 Q_{n_1\kappa_1}(r_1) \\
& \times P_{\epsilon_2\kappa_2}(r_2) QP^{1M}_{\kappa_1\kappa_2}(r_1, r_2, t \to \infty) \\
& + \int_0^\infty \mathrm{d}r_1 \int_0^\infty \mathrm{d}r_2 P_{n_1\kappa_1}(r_1) \\
& \times Q_{\epsilon_2\kappa_2}(r_2) PQ^{1M}_{\kappa_1\kappa_2}(r_1, r_2, t \to \infty) \\
& + \int_0^\infty \mathrm{d}r_1 \int_0^\infty \mathrm{d}r_2 Q_{n_1\kappa_1}(r_1) \\
& \times Q_{\epsilon_2\kappa_2}(r_2) QQ^{1M}_{\kappa_1\kappa_2}(r_1, r_2, t \to \infty)|^2,
\end{aligned} \tag{28}$$

where $P_{n\kappa}(r)$ and $Q_{n\kappa}(r)$ are bound states and $P_{\epsilon\kappa}(r)$ and $Q_{\epsilon\kappa}(r)$ are continuum states of the positive energy solutions

obtained by diagonalization of the one-electron radial Dirac equation given by:

$$\begin{pmatrix} -\frac{Z}{r} - 2c^2 & c(\frac{\partial}{\partial r} + \frac{\kappa}{r}) \\ -c(\frac{\partial}{\partial r} - \frac{\kappa}{r}) & -\frac{Z}{r} \end{pmatrix} \begin{pmatrix} Q_{\epsilon\kappa}(r) \\ P_{\epsilon\kappa}(r) \end{pmatrix} = \epsilon \begin{pmatrix} Q_{\epsilon\kappa}(r) \\ P_{\epsilon\kappa}(r) \end{pmatrix}. \quad (29)$$

The single photoionization cross section leaving the ion in state $n_1\kappa_1$ is given by:

$$\sigma_{\text{single}}(n_1\kappa_1) = \frac{\omega}{IT}\mathcal{P}_s(n_1\kappa_1), \quad (30)$$

where I is the field intensity and T is the total elapsed time for a constant intensity pulse. The total single photoionization cross section is given by:

$$\sigma_{\text{single}} = \sum_{n_1\kappa_1} \sigma_{\text{single}}(n_1\kappa_1). \quad (31)$$

The double photoionization probability is given by:

$$\begin{aligned} \mathcal{P}_d = \sum_M \sum_{\epsilon_1\kappa_1} \sum_{\epsilon_2\kappa_2} \Bigg| & \int_0^\infty dr_1 \int_0^\infty dr_2 P_{\epsilon_1\kappa_1}(r_1) \\ & \times P_{\epsilon_2\kappa_2}(r_2) PP^{1M}_{\kappa_1\kappa_2}(r_1, r_2, t \to \infty) \\ & + \int_0^\infty dr_1 \int_0^\infty dr_2 Q_{\epsilon_1\kappa_1}(r_1) \\ & \times P_{\epsilon_2\kappa_2}(r_2) QP^{1M}_{\kappa_1\kappa_2}(r_1, r_2, t \to \infty) \\ & + \int_0^\infty dr_1 \int_0^\infty dr_2 P_{\epsilon_1\kappa_1}(r_1) \\ & \times Q_{\epsilon_2\kappa_2}(r_2) PQ^{1M}_{\kappa_1\kappa_2}(r_1, r_2, t \to \infty) \\ & + \int_0^\infty dr_1 \int_0^\infty dr_2 Q_{\epsilon_1\kappa_1}(r_1) \\ & \times Q_{\epsilon_2\kappa_2}(r_2) QQ^{1M}_{\kappa_1\kappa_2}(r_1, r_2, t \to \infty) \Bigg|^2. \end{aligned} \quad (32)$$

The double photoionization cross section is given by:

$$\sigma_{\text{double}} = \frac{\omega}{IT}\mathcal{P}_d. \quad (33)$$

3. Results

To obtain a complete set of positive and negative energy solutions for Ne^{9+}, we first diagonalized the Hamiltonian of equation (29) with $\kappa = -1, +1, -2, +2, -3, +3$. With $Z = 10$ we used a 480 point radial mesh with $\Delta r = 0.01$. To avoid the Fermi doubling pathology [21] we used a fifth order forward differencing scheme for $\frac{\partial Q(r)}{\partial r}$ and a fifth order backward differencing scheme for $\frac{\partial P(r)}{\partial r}$. The 480 negative energy eigenfunctions for $\kappa = -1$ are found to have energies ranging from -1.63 MeV to -1.02 MeV. The 480 positive energy eigenfunctions for $\kappa = -1$ are found to have energies ranging from -1.3 keV to $+0.61$ MeV.

For the fully correlated ground state of Ne^{8+}, we solved the close-coupled equations associated with equation (23) using the 6 coupled channels found in table 1 for $J = 0, M = 0$. We used a 480×480 point numerical lattice with $\Delta r_1 = \Delta r_2 = 0.01$, with each radial mesh partitioned over 48 core processors on a massively parallel supercomputer. The radial wavefunction associated with $\vec{\Psi}_0(\vec{r}_1, \vec{r}_2)$ is taken as the quad-spinor given by:

$$\Psi_0(r_1, r_2) = \begin{pmatrix} P_{1s\frac{1}{2}}(r_1) P_{1s\frac{1}{2}}(r_2) \\ Q_{1rms\frac{1}{2}}(r_1) P_{1s\frac{1}{2}}(r_2) \\ P_{1s\frac{1}{2}}(r_1) Q_{1s\frac{1}{2}}(r_2) \\ Q_{1s\frac{1}{2}}(r_1) Q_{1s\frac{1}{2}}(r_2) \end{pmatrix}, \quad (34)$$

Table 1. Initial state coupled channels ($J = 0$).

Channel	l_1	j_1	κ_1	l_2	j_2	κ_2
1	s	$\frac{1}{2}$	-1	s	$\frac{1}{2}$	-1
2	p	$\frac{1}{2}$	$+1$	p	$\frac{1}{2}$	$+1$
3	p	$\frac{3}{2}$	-2	p	$\frac{3}{2}$	-2
4	d	$\frac{3}{2}$	$+2$	d	$\frac{3}{2}$	$+2$
5	d	$\frac{5}{2}$	-3	d	$\frac{5}{2}$	-3
6	f	$\frac{5}{2}$	$+3$	f	$\frac{5}{2}$	$+3$

Table 2. Final state coupled channels ($J = 1$).

Channel	l_1	j_1	κ_1	l_2	j_2	κ_2
1	s	$\frac{1}{2}$	-1	p	$\frac{1}{2}$	$+1$
2	p	$\frac{1}{2}$	$+1$	s	$\frac{1}{2}$	-1
3	s	$\frac{1}{2}$	-1	p	$\frac{3}{2}$	-2
4	p	$\frac{3}{2}$	-2	s	$\frac{1}{2}$	-1
5	p	$\frac{1}{2}$	$+1$	d	$\frac{3}{2}$	$+2$
6	d	$\frac{3}{2}$	$+2$	p	$\frac{1}{2}$	$+1$
7	p	$\frac{3}{2}$	-2	d	$\frac{3}{2}$	$+2$
8	d	$\frac{3}{2}$	$+2$	p	$\frac{3}{2}$	-2
9	p	$\frac{3}{2}$	-2	d	$\frac{5}{2}$	-3
10	d	$\frac{5}{2}$	-3	p	$\frac{3}{2}$	-2
11	d	$\frac{3}{2}$	$+2$	f	$\frac{5}{2}$	$+3$
12	f	$\frac{5}{2}$	$+3$	d	$\frac{3}{2}$	$+2$
13	d	$\frac{5}{2}$	-3	f	$\frac{5}{2}$	$+3$
14	f	$\frac{5}{2}$	$+3$	d	$\frac{5}{2}$	-3

where $P_{1s\frac{1}{2}}(r)$ and $Q_{1s\frac{1}{2}}(r)$ are obtained from the diagonalization of equation (29) with $\kappa = -1$. The approximate ground state energy in equation (23) is given by:

$$E_0 = \langle \vec{\Psi}_0(\vec{r}_1, \vec{r}_2) | \bar{H}(\vec{r}_1, \vec{r}_2) | \vec{\Psi}_0(\vec{r}_1, \vec{r}_2) \rangle, \quad (35)$$

where $\bar{H}(\vec{r}_1, \vec{r}_2)$ is again found from equation (2) with $U_i(t) = 0$ and $\vec{A}_i(t) = 0$.

In solving the inhomogeneous Dirac equation for Ne^{8+}, we used a uniform time mesh of $\Delta t = 1.0 \times 10^{-5}$ and a homing time of $T_0 = 1.00$. After 100 000 time steps the ground state energy for Ne^{8+} was found to be -2.4604 keV when only the Coulomb interaction was included, and -2.4600 keV when both the Coulomb and Gaunt interactions were included. The slight change in total energy due to the Gaunt interaction is in good agreement with GRASP calculations (see chapter 7) [4] for a Breit interaction contribution of +0.33 eV. For a homing time of $T_0 = 1.50$ and 150 000 time steps, the ground state energies for Ne^{8+} remained the same. We note that by reducing the radial mesh spacings Δr_1 and Δr_2 we obtain absolute ground state energies that approach the experimental value. Fortunately, the fine mesh is not needed to obtain accurate photoionization cross sections.

To obtain photoionization cross sections we solved the TDCC-6D equations given by equations (10)– (13). For dipole only interactions we used the 20 coupled channels found in table 1 for $J = 0, M = 0$ and in table 2 for $J = 1, M = 0$. For dipole and quadrupole interactions we used the 42 coupled

Table 3. Final state coupled channels ($J = 2$).

Channel	l_1	j_1	κ_1	l_2	j_2	κ_2
1	s	$\frac{1}{2}$	-1	d	$\frac{3}{2}$	$+2$
2	d	$\frac{3}{2}$	$+2$	s	$\frac{1}{2}$	-1
3	s	$\frac{1}{2}$	-1	d	$\frac{5}{2}$	-3
4	d	$\frac{5}{2}$	-3	s	$\frac{1}{2}$	-1
5	p	$\frac{1}{2}$	$+1$	p	$\frac{3}{2}$	-2
6	p	$\frac{3}{2}$	-2	p	$\frac{1}{2}$	$+1$
7	p	$\frac{3}{2}$	-2	p	$\frac{3}{2}$	-2
8	p	$\frac{1}{2}$	$+1$	f	$\frac{5}{2}$	$+3$
9	f	$\frac{5}{2}$	$+3$	p	$\frac{1}{2}$	$+1$
10	p	$\frac{3}{2}$	-2	f	$\frac{5}{2}$	$+3$
11	f	$\frac{5}{2}$	$+3$	p	$\frac{3}{2}$	-2

Table 4. Photoionization cross sections for Ne^{8+} including only dipole and Coulomb interactions. (1.0 Kb = 1.0×10^{-21} cm^2 and 1.0 b = 1.0×10^{-24} cm^2.)

Photon energy (eV)	σ_{single} (Kb)	σ_{double} (b)
2500.0	21.91	2.73
2750.0	16.63	9.43
3000.0	13.02	11.90
3500.0	8.39	11.09
4000.0	5.67	8.67
5000.0	2.97	4.89
6000.0	1.70	2.81
7000.0	1.09	1.71
8000.0	0.74	1.09
9000.0	0.52	0.73
10 000.0	0.38	0.51

channels found in table 1 for $J = 0, M = 0$, in table 2 for $J = 1, M = 0$, and in table 3 for $J = 2, M = \pm 1$. We again used a 480×480 point numerical lattice with $\Delta r_1 = \Delta r_2 = 0.01$, with each radial mesh partitioned over 48 core processors on a massively parallel supercomputer. Single and double photoionization probabilities were calculated using equations (28) and (32), which involve integrals over the time propagated coupled channel radial functions, all the bound single particle positive energy solutions, and the lowest 40 continuum single particle positive energy solutions. Single and double photoionization cross sections were calculated using equations (31) and (33).

For Ne^{8+} we used an intensity of 10^{15} Watts cm^{-2} while propagating the TDCC-6D equations for ten radiation field periods with a uniform time mesh of $\Delta t = 1.0 \times 10^{-5}$. Since the 'length' gauge emphasizes larger distances from the nuclear charge, it is more accurate for uniform mesh lattice calculations and is thus used for all the Ne^{8+} calculations. Including only dipole and Coulomb interactions, single and double photoionization cross sections over a range of photon energies from near threshold to 10 000 eV are presented in table 4. Including dipole, quadrupole, Coulomb, and Gaunt interactions, single and double photoionization cross sections are presented in table 5. For the relatively low charged Ne^{8+} atomic ion, the quadrupole and Gaunt interactions yield only a slight increase in the single and double photoionization cross sections.

Table 5. Photoionization cross sections for Ne^{8+} including dipole, quadrupole, Coulomb, and Gaunt interactions. (1.0 Kb = 1.0×10^{-21} cm^2 and 1.0 b = 1.0×10^{-24} cm^2.)

Photon energy (eV)	σ_{single} (Kb)	σ_{double} (b)
2500.0	22.01	2.78
2750.0	16.71	9.55
3000.0	13.10	12.07
3500.0	8.46	11.28
4000.0	5.72	8.86
5000.0	3.01	5.04
6000.0	1.73	2.93
7000.0	1.11	1.80
8000.0	0.76	1.16
9000.0	0.54	0.79
10 000.0	0.39	0.56

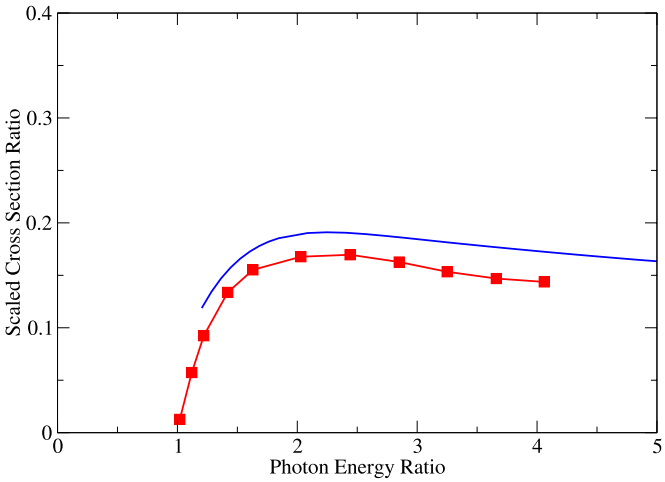

Figure 1. Photon-impact double to single ionization cross section ratios for Ne^{8+}. The scaled cross section ratio is $100\,\sigma_{\text{single}}(1s\frac{1}{2})/\sigma_{\text{double}}$ and the scaled photon energy ratio is $\omega/2460$ for ω in eV. Connected solid (red) squares: TDCC-6D calculations, solid (blue) curve: fully-relativistic perturbation theory calculations [5].

The TDCC-6D calculations including dipole, quadrupole, Coulomb, and Gaunt interactions are compared with fully relativistic perturbation theory calculations [5] for the scaled cross section ratio:

$$R = \frac{Z^2 \sigma_{\text{single}}(1s\frac{1}{2})}{\sigma_{\text{double}}} \tag{36}$$

versus photon energy ratio (ω/ω_t) with $Z = 10$ and $\omega_t = 2460$ eV in figure 1. The TDCC-6D cross section ratios are found to be 10% to 15% below the perturbation theory ratios, but follow the same trend with photon energy ratio. We note that the accurate calculation of double ionization cross sections is difficult using perturbation theory. The TDCC-6D calculations including dipole, quadrupole, Coulomb, and Gaunt interactions are compared with recent intermediate energy R-matrix (IERM) calculations [22] for the double ionization cross section in figure 2. Overall there is good agreement between the two non-perturbative calculations. For the relatively low charged Ne^{8+} atomic ion, the IERM results for the double ionization cross sections should be quite accurate.

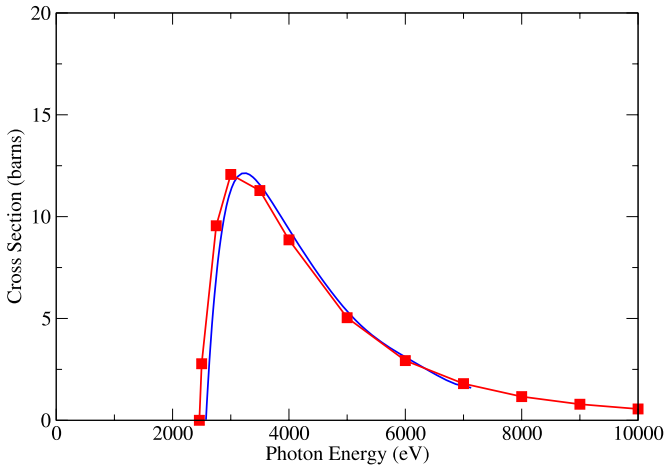

Figure 2. Photon-impact double ionization of Ne^{8+}. Solid (red) curve with squares: TDCC-6D calculations, solid (blue) curve : IERM calculations [22] (1.0 barn = 1.0×10^{-24} cm^2).

4. Summary

Using the Dirac equation with a full electromagnetic field potential in both the 'velocity' and 'length' gauges, relativistic time-dependent close-coupled equations were derived for the single and double photoionization of two active electron atomic ions. Key steps in the derivation are the introduction of an expansion in spherical Bessel functions for the electromagnetic field operators and algebraic reduction of the jjJ coupled state matrix elements of the associated tensor operators. Algebraic reduction of the jjJ coupled state matrix elements was also made for the tensor operators associated with the Coulomb and Gaunt two-body interactions. A key step in obtaining a well-behaved time evolution of a two electron system interacting with an electromagnetic field is the introduction of an inhomogeneous Dirac equation method for calculation of the fully correlated initial ground state. The single and double photoionization cross sections for Ne^{8+} were calculated over an energy range easily accessible at advanced free electron facilities and were found to be in reasonably good agreement with fully-relativistic distorted-wave and non-perturbative IERM results.

In the future, we plan to apply the fully-relativistic TDCC-6D method to look at double photoionization energy and angle differential cross sections. Perturbation theory breaks down completely for two electrons moving in the same direction at close to the same energies. We also plan to look for exotic effects of the underlying Dirac sea of negative energy solutions on the double photoionization cross sections as we move to more highly charged atomic ions.

Acknowledgments

This work was supported in part by grants from the US Department of Energy and the US National Science Foundation. Computational work was carried out at the National Energy Research Scientific Computing Center in Oakland, California and the National Institute for Computational Sciences in Knoxville, Tennessee.

Appendix

Matrix elements involving the radiation field for coordinate $\vec{r}_1$ are given by:

$$\begin{aligned}
&\langle(\kappa_1,\kappa_2)JM|S^1_0|(\kappa'_1,\kappa'_2)J'M'\rangle \\
&\quad=\delta_{l_2,l'_2}\delta_{j_2,j'_2}\delta_{l_1,l'_1}(-1)^{J+J'-M+2j_1+j_2+l_1+\frac{1}{2}} \\
&\qquad\times\sqrt{3/2}\sqrt{(2J+1)(2J'+1)(2j_1+1)(2j'_1+1)} \\
&\qquad\times\begin{pmatrix} J & 1 & J' \\ -M & 0 & M' \end{pmatrix}\begin{Bmatrix} j_1 & j_2 & J \\ J' & 1 & j'_1 \end{Bmatrix}\begin{Bmatrix} l_1 & \frac{1}{2} & j_1 \\ 1 & j'_1 & \frac{1}{2} \end{Bmatrix}, \qquad \text{(A.1)}
\end{aligned}$$

$$\begin{aligned}
&\langle(\kappa_1,\kappa_2)JM|C^1_0|(\kappa'_1,\kappa'_2)J'M'\rangle=\delta_{l_2,l'_2}\delta_{j_2,j'_2} \\
&\qquad\times(-1)^{J+J'-M+j_1+j'_1+j_2+\frac{1}{2}} \\
&\qquad\times\sqrt{(2l_1+1)(2l'_1+1)}\begin{pmatrix} l_1 & 1 & l'_1 \\ 0 & 0 & 0 \end{pmatrix} \\
&\qquad\times\sqrt{(2J+1)(2J'+1)(2j_1+1)(2j'_1+1)} \\
&\qquad\times\begin{pmatrix} J & 1 & J' \\ -M & 0 & M' \end{pmatrix}\begin{Bmatrix} j_1 & j_2 & J \\ J' & 1 & j'_1 \end{Bmatrix}\begin{Bmatrix} l_1 & \frac{1}{2} & j_1 \\ j'_1 & 1 & l'_1 \end{Bmatrix}, \qquad \text{(A.2)}
\end{aligned}$$

and

$$\begin{aligned}
&\langle(\kappa_1,\kappa_2)JM|V(k)^K_Q|(\kappa'_1,\kappa'_2)J'M'\rangle=\delta_{l_2,l'_2}\delta_{j_2,j'_2} \\
&\qquad\times(-1)^{J+J'-M+j_1+j_2+l_1+K}\sqrt{3/2(2K+1)} \\
&\qquad\times\sqrt{(2l_1+1)(2l'_1+1)}\begin{pmatrix} l_1 & k & l'_1 \\ 0 & 0 & 0 \end{pmatrix} \\
&\qquad\times\sqrt{(2J+1)(2J'+1)(2j_1+1)(2j'_1+1)} \\
&\qquad\times\begin{pmatrix} J & K & J' \\ -M & Q & M' \end{pmatrix}\begin{Bmatrix} j_1 & j_2 & J \\ J' & K & j'_1 \end{Bmatrix}\begin{Bmatrix} l_1 & \frac{1}{2} & j_1 \\ l'_1 & \frac{1}{2} & j'_1 \\ k & 1 & K \end{Bmatrix}. \qquad \text{(A.3)}
\end{aligned}$$

Matrix elements involving the radiation field for coordinate $\vec{r}_2$ are given by:

$$\begin{aligned}
&\langle(\kappa_1,\kappa_2)JM|S^1_0|(\kappa'_1,\kappa'_2)J'M'\rangle=\delta_{l_1,l'_1}\delta_{j_1,j'_1}\delta_{l_2,l'_2} \\
&\qquad\times(-1)^{2J-M+j_1+j_2+j'_2+l_2+\frac{1}{2}} \\
&\qquad\times\sqrt{3/2}\sqrt{(2J+1)(2J'+1)(2j_2+1)(2j'_2+1)} \\
&\qquad\times\begin{pmatrix} J & 1 & J' \\ -M & 0 & M' \end{pmatrix}\begin{Bmatrix} j_1 & j_2 & J \\ 1 & J' & j'_2 \end{Bmatrix}\begin{Bmatrix} l_2 & \frac{1}{2} & j_2 \\ 1 & j'_2 & \frac{1}{2} \end{Bmatrix}, \qquad \text{(A.4)}
\end{aligned}$$

$$\begin{aligned}
&\langle(\kappa_1,\kappa_2)JM|C^1_0|(\kappa'_1,\kappa'_2)J'M'\rangle=\delta_{l_1,l'_1}\delta_{j_1,j'_1} \\
&\qquad\times(-1)^{2J-M+j_1+j_2+2j'_2+\frac{1}{2}} \\
&\qquad\times\sqrt{(2l_2+1)(2l'_2+1)}\begin{pmatrix} l_2 & 1 & l'_2 \\ 0 & 0 & 0 \end{pmatrix} \\
&\qquad\times\sqrt{(2J+1)(2J'+1)(2j_2+1)(2j'_2+1)} \\
&\qquad\begin{pmatrix} J & 1 & J' \\ -M & 0 & M' \end{pmatrix}\begin{Bmatrix} j_1 & j_2 & J \\ 1 & J' & j'_2 \end{Bmatrix}\begin{Bmatrix} l_2 & \frac{1}{2} & j_2 \\ j'_2 & 1 & l'_2 \end{Bmatrix}, \qquad \text{(A.5)}
\end{aligned}$$

and

$$\begin{aligned}
&\langle(\kappa_1,\kappa_2)JM|V(k)^K_Q|(\kappa'_1,\kappa'_2)J'M'\rangle=\delta_{l_1,l'_1}\delta_{j_1,j'_1} \\
&\qquad\times(-1)^{2J-M+j_1+j'_2+l_2+K}\sqrt{3/2(2K+1)} \\
&\qquad\times\sqrt{(2l_2+1)(2l'_2+1)}\begin{pmatrix} l_2 & k & l'_2 \\ 0 & 0 & 0 \end{pmatrix}
\end{aligned}$$

$$\times\sqrt{(2J+1)(2J'+1)(2j_2+1)(2j_2'+1)}$$
$$\times\begin{pmatrix} J & K & J' \\ -M & Q & M' \end{pmatrix}\begin{Bmatrix} j_1 & j_2 & J \\ K & J' & j_2' \end{Bmatrix}\begin{Bmatrix} l_2 & \frac{1}{2} & j_2 \\ l_2' & \frac{1}{2} & j_2' \\ k & 1 & K \end{Bmatrix}. \quad \text{(A.6)}$$

Matrix elements involving the two-body Coulomb interaction are given by:

$$\langle(\kappa_1,\kappa_2)JM|C(\vec{r}_1,\vec{r}_2)|(\kappa_1',\kappa_2')J'M'\rangle$$
$$= (-1)^{2j_1'+j_2+j_2'+J+1}\delta_{J,J'}\delta_{M,M'}$$
$$\times\sqrt{(2l_1+1)(2l_1'+1)(2l_2+1)(2l_2'+1)}$$
$$\times\sqrt{(2j_1+1)(2j_1'+1)(2j_2+1)(2j_2'+1)}$$
$$\times\sum_{\lambda}\frac{r_<^{\lambda}}{r_>^{\lambda+1}}\begin{pmatrix} l_1 & \lambda & l_1' \\ 0 & 0 & 0 \end{pmatrix}\begin{pmatrix} l_2 & \lambda & l_2' \\ 0 & 0 & 0 \end{pmatrix}$$
$$\times\begin{Bmatrix} l_1 & \frac{1}{2} & j_1 \\ j_1' & \lambda & l_1' \end{Bmatrix}\begin{Bmatrix} l_2 & \frac{1}{2} & j_2 \\ j_2' & \lambda & l_2' \end{Bmatrix}\begin{Bmatrix} j_1 & j_2 & J \\ j_2' & j_1' & \lambda \end{Bmatrix}. \quad \text{(A.7)}$$

Matrix elements involving the two-body Gaunt interaction are given by:

$$\langle(\kappa_1,\kappa_2)JM|G(\vec{r}_1,\vec{r}_2)|(\kappa_1',\kappa_2')J'M'\rangle$$
$$= (-1)^{j_1'+j_2+J+l_1+l_2}4(3/2)\delta_{J,J'}\delta_{M,M'}$$
$$\times\sqrt{(2l_1+1)(2l_1'+1)(2l_2+1)(2l_2'+1)}$$
$$\times\sqrt{(2j_1+1)(2j_1'+1)(2j_2+1)(2j_2'+1)}$$
$$\times\sum_{\lambda,K}(-1)^{\lambda+K}(2K+1)\frac{r_<^{\lambda}}{r_>^{\lambda+1}}\begin{pmatrix} l_1 & \lambda & l_1' \\ 0 & 0 & 0 \end{pmatrix}\begin{pmatrix} l_2 & \lambda & l_2' \\ 0 & 0 & 0 \end{pmatrix}$$
$$\times\begin{Bmatrix} j_1 & j_2 & J \\ j_2' & j_1' & K \end{Bmatrix}\begin{Bmatrix} l_1 & \frac{1}{2} & j_1 \\ l_1' & \frac{1}{2} & j_1' \\ \lambda & 1 & K \end{Bmatrix}\begin{Bmatrix} l_2 & \frac{1}{2} & j_2 \\ l_2' & \frac{1}{2} & j_2' \\ \lambda & 1 & K \end{Bmatrix}. \quad \text{(A.8)}$$

References

[1] FLASH http://flash.desy.de
[2] LCLS http://lcls.slac.stanford.edu
[3] XFEL http://xfel.desy.de
[4] Grant I P 2007 *Relativistic Quantum Theory of Atoms and Molecules* (New York: Springer)
[5] Yerokhin V A and Surzhykov A 2011 *Phys. Rev.* A **84** 032703
[6] Norrington P H and Grant I P 1981 *J. Phys. B: At. Mol. Phys.* **14** L261
[7] Zatsarinny O and Bartschat K 2008 *Phys. Rev.* A **77** 062701
[8] Bostock C J, Fursa D V and Bray I 2012 *Phys. Rev.* A **86** 042709
[9] Badnell N R 2008 *J. Phys. B: At. Mol. Opt. Phys.* **41** 175202
[10] Selsto S, Lindroth E and Bengtsson J 2009 *Phys. Rev.* A **79** 043418
[11] Pindzola M S, Abdel-Naby S A, Robicheaux F and Colgan J 2012 *Phys. Rev.* A **85** 032701
[12] Pindzola M S, Ludlow J A and Colgan J 2010 *Phys. Rev.* A **81** 063431
[13] Dirac P A M 1928 *Proc. R. Soc.* A **117** 610
[14] Breit G 1929 *Phys. Rev.* **34** 553
[15] Cohen-Tannoudji C, Diu B and Laloe F 1977 *Quantum Mechanics* (New York: Wiley)
[16] Gaunt J A 1929 *Proc. R. Soc.* A **122** 513
[17] Mann J B and Johnson W R 1971 *Phys. Rev.* A **4** 41
[18] Cowan R D 1981 *The Theory of Atomic Structure and Spectra* (Berkeley: University of California)
[19] Topcu T 2007 Time-dependent studies of fundamental atomic processes in Rydberg atoms *PhD Thesis* Auburn University, AL
[20] Bottcher C, Strayer M R, Umar A S and Reinhard P G 1989 *Phys. Rev.* A **40** 4182
[21] Bottcher C and Strayer M R 1987 *Ann. Phys.* **175** 64
[22] McIntyre M W, Kinnen A J and Scott M P 2013 *Phys. Rev.* A **88** 053413